Pacific Graphics 2009
S. Lee, D. Lischinski, and Y. Yu
(Guest Editors)

Volume 28 (*2009*), *Number 7*

Generalized Discrete Ricci Flow

Yong-Liang Yang[1] Ren Guo[2] Feng Luo[2] Shi-Min Hu[1] Xianfeng Gu[3]

[1]Tsinghua National Laboratory for Information Science and Technology
Department of Computer Science and Technology, Tsinghua University
[2]Department of Mathematics, Rutgers University
[3]Department of Computer Science, Stony Brook University

Abstract

Surface Ricci flow is a powerful tool to design Riemannian metrics by user defined curvatures. Discrete surface Ricci flow has been broadly applied for surface parameterization, shape analysis, and computational topology. Conventional discrete Ricci flow has limitations. For meshes with low quality triangulations, if high conformality is required, the flow may get stuck at the local optimum of the Ricci energy. If convergence to the global optimum is enforced, the conformality may be sacrificed.
This work introduces a novel method to generalize the traditional discrete Ricci flow. The generalized Ricci flow is more flexible, more robust and conformal for meshes with low quality triangulations. Conventional method is based on circle packing, which requires two circles on an edge intersect each other at an acute angle. Generalized method allows the two circles either intersect or separate from each other. This greatly improves the flexibility and robustness of the method. Furthermore, the generalized Ricci flow preserves the convexity of the Ricci energy, this ensures the uniqueness of the global optimum. Therefore the algorithm won't get stuck at the local optimum.
Generalized discrete Ricci flow algorithms are explained in details for triangle meshes with both Euclidean and hyperbolic background geometries. Its advantages are demonstrated by theoretic proofs and practical applications in graphics, especially surface parameterization.

Categories and Subject Descriptors (according to ACM CCS): I.3.5 [Computer Graphics]: Computational Geometry and Object Modeling —Geometric algorithms, languages, and systems

1. Introduction

1.1. Ricci Flow and Applications

Ricci flow is a powerful tool to design Riemannian metrics using user defined curvatures. Intuitively, Ricci flow deforms a Riemannian metric proportional to the curvature. The deformed metric will change the curvature, such that the curvature evolves according to a heat diffusion process. Eventually the curvature becomes constant everywhere. Moreover, Ricci flow is the gradient flow of a special energy form - *entropy*, the metric with constant curvature is the global optimum of the entropy.

Surface Ricci flow has broad applications in graphics field, in the following, we only briefly introduce a few most related examples. *Surface parameterization* refers to the process to map the surface onto a planar domain, which can be formulated as designing a Riemannian metric of the surface, such that all the interior points are with zero Gaussian curvatures, namely a flat metric. By changing the geodesic curvatures on the boundary points, the flat metric will be changed accordingly. By adjusting the boundary geodesic curvatures, an optimal parameterization can be achieved, which minimizes the distortion [YKL*08]. In *computational topology*, Ricci flow has been applied to compute the canonical representative in each homotopy class of loops [ZJLG09]. Two loops are homotopic, if one can deform to the other on the surface. If the surface has a Riemannian metric with negative Gaussian curvature, then each homotopy class has a unique closed geodesic. Given a high genus surface, Ricci flow is used to compute the metric with -1 Gaussian curvature (hyperbolic metric). Then the closed geometric loop can be computed in each homotopy class, which is the canonical representative of the class. Ricci flow has also been applied to the *shape space* [JZLG08]. Two surfaces are conformal equivalent, if there is an angle-preserving map between them. All surfaces in $\mathbb{R}^3$ can be classified by the conformal equivalence relation. All the conformal equivalence classes form a finite dimensional Riemannian manifold, where each

point represents a class of surfaces, a curve represent a deformation process. Given a surface in $\mathbb{R}^3$, its coordinates in this shape space can be computed using Ricci flow.

1.2. Generalization of Discrete Ricci Flow

Ricci flow deforms a Riemannian metric on the surface in an *angle-preserving* manner, namely, the metric deformation is *conformal*. Locally, conformal metric deformation transforms an infinitesimal circle to an infinitesimal circle. Fig. 1 illustrates the property of Ricci flow. The Stanford bunny is embedded in $\mathbb{R}^3$, it has an induced Euclidean metric. By using Ricci flow, the metric is conformally deformed to a flat metric (with cone singularities), all Gaussian curvatures are zeros, then the bunny surface is flattened onto the plane. The planar circle packing texture shown in the upper right corner is mapped onto the surface. All the planar circles are mapped to circles, the tangential relations are preserved. This property inspires Thurston [Thu80] to invent discrete conformal mapping using *circle packing metric* as shown in Fig. 2. Given a planar domain in frame (a), we triangulate the domain. Then we put a circle at each vertex, and all circles are tangent to each other. Then we change the circle radii, and keep the tangential relations. This will deform the domain to different planar domains as shown in frame (b) and (c). The piecewise linear mapping is a discrete conformal mapping. If we refine the triangulation, such that the diameter of each triangle goes to zero, then the discrete conformal mapping will converge to the real conformal mapping under some normalization conditions. The theoretic proof is given by He et.al. [xHS96].

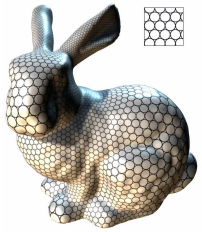

Figure 1: *Conformal metric deformation maps infinitesimal circles to infinitesimal circles.*

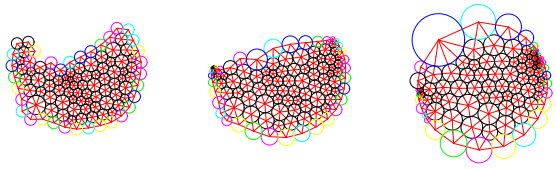

(a) (b) (c)

Figure 2: *Thurston's discrete conformal deformation using circle packing metric.*

Thurston's circle packing method is too restrictive. Later it is generalized from planar domains to surface domains. Furthermore, the circles can intersect each other with acute angles. Fig. 3 shows the circle packing on one triangle. Two circles at the vertices of an edge intersect each other with an acute intersection angle. The circle radii can be modified, but the intersection angles are preserved. This gives us the discrete conformal metric deformation for surfaces. Chow and Luo [CL03] built the intrinsic relation between discrete conformal metric deformation and surface Ricci flow. They showed that the discrete Ricci flow is stable and leads to the unique solution, as long as all the intersection angles (ϕ_{ij} in Fig. 3) are acute. If the intersection angles are obtuse, the solution may not be unique, the discrete curvature flow may get stuck at the local optimum.

Unfortunately, in reality, the acute intersection angle condition is too restrictive. Triangle meshes obtained from raw scan data or reconstructed using marching cubes method, such as [Ju04], always have skinny triangles. The Kitten mesh in Fig. 4 is reconstructed using marching cubes method [Ju04]. Fig. 4(b) shows a local region near the nose. It is clear that there are many triangles nearly being degenerated.

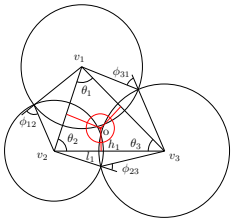

Figure 3: *Conventional discrete Ricci flow.*

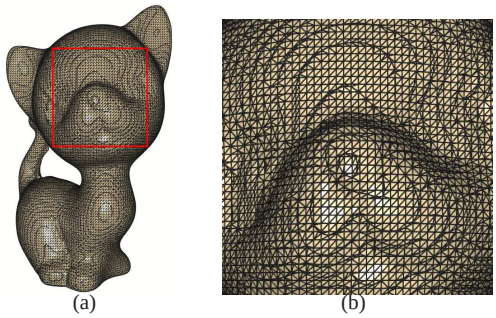

(a) (b)

Figure 4: *Kitten model is re-triangulated using Polymender in [Ju04], which has skinny triangles.*

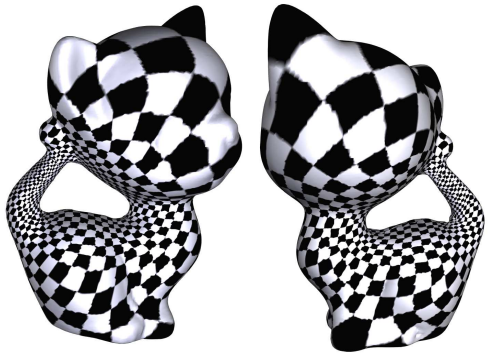

Figure 5: *Bad conformality of traditional discrete surface Ricci flow on meshes with low quality triangulations.*

It is hardly to find a circle packing on the mesh, such that all

the intersection angles are acute. In order to ensure the convergence of the curvature flow, the intersection angles are forced to be acute. Therefore, the circle packing metric is no longer consistent with the original induced Euclidean metric of the mesh. The conformality of the final mapping is compromised. Fig. 5 shows the low conformality of the surface parameterization using conventional Ricci flow method on the mesh with low quality of triangulation. Note that for conventional Ricci flow, there might be an optional preprocessing step to re-triangulate the input mesh [YKL*08], such that the circle packing metric and the Euclidean metric can be more consistent.

In order to achieve high conformality even on meshes with bad triangulations, this work generalizes the traditional circle packing metric shown in Fig. 3 to *inversive distance circle packing* in Fig. 6. The conventional Ricci flow requires all the intersection angles to be acute. The generalized Ricci flow relaxes the acute intersection angle condition, such that two circles on an edge either intersect at an acute angle or separate from each other. It is guaranteed that given arbitrary triangular mesh with an initial induced Euclidean metric, a generalized circle packing can be found, such that the circle packing metric is consistent with the induced Euclidean metric. Therefore, the generalized Ricci flow method guarantees high conformality. Furthermore, we can show that the generalized Ricci flow is the gradient flow of a convex energy. There exists a unique global optimum, the generalized flow leads to the unique solution. In one word, the generalized Ricci flow is flexible, robust and conformal to meshes with bad triangulations. Fig. 7 shows the parameterization result of the same Kitten mesh in Fig. 4 with high conformality. Comparing with Fig. 5, it is obvious that the generalized Ricci flow has enormously improved the conformality.

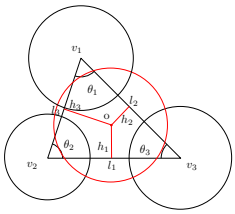

Figure 6: *Inversive distance discrete Ricci flow.*

1.3. Contributions

Compared to traditional discrete Ricci flow [JKLG08], this work has the following major contributions:

1. Generalizes discrete Euclidean Ricci flow (Fig. 3) to include inversive distance circle packing (Fig. 6), while the traditional one requires two circles on an edge intersect each other at an acute angle. This will help to largely improve the conformality of the parameterization result on meshes with low quality triangulations.
2. Explicitly gives the geometric meaning of the Hessian matrix of discrete Euclidean Ricci energy (see Lemma 3.7 and the appendix for the proof). In [JKLG08], the Hessian matrix has more complicated form because it is derived by explicit computation of the discrete Ricci energy.
3. Generalizes discrete hyperbolic Ricci flow (Fig. 3) to include inversive distance circle packing (Fig. 6).

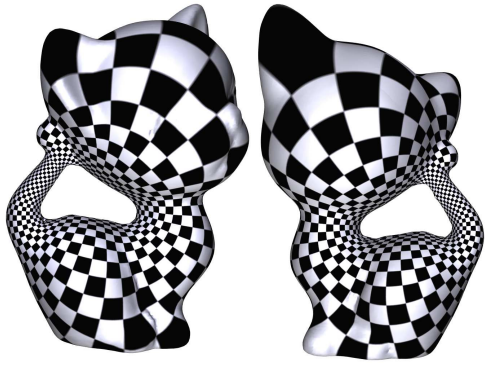

Figure 7: *High conformality of generalized discrete surface Ricci flow on meshes with low quality triangulations.*

We show that both the discrete Euclidean Ricci energy and the hyperbolic Ricci energy are convex. Therefore, the generalized Ricci flow converges to the unique solution, which is the global optimum of the Ricci energy. The Ricci energy can be efficiently optimized using Newton's method.

1.4. Organizations

Section 2 briefly reviews the most related works. Section 3 explains the discrete genearlized Ricci flow for both Euclidean case and hyperbolic case. Section 4 introduces the algorithms in details. Experimental results are reported in Section 5. The paper is concluded in Section 6.

2. Previous Works

2.1. Mesh Parameterization

Mesh parameterization has been an active research topic in geometry processing, it is also a fundamental tool widely used in graphics field. Here we only briefly review the most related works and refer readers to [FH05, SPR06, HLS07] for more thorough surveys.

The aim of parameterization is to build a map (ideally one-to-one) from the mesh surface to 2D planar domain. Early parameterization methods [EDD*95, Flo97] treat interior mesh vertex as some convex combination of its neighboring vertices based on Tutte's embedding theorem [Tut63]. Taking mesh geometry into account, the simple graph Laplacian is extended to the well-known cotangent weights [PP93] and mean value coordinates [Flo03]. These methods generally require fixing mesh boundary onto a convex planar shape to make the mapping bijective, which usually provides parameterization results with large area distortion. Boundary free parameterization is then proposed as an energy minimization problem in [LPRM02] and [DMA02].

The former one approximates the Cauchy-Riemann equation and the latter optimizes Dirichlet energy. These two methods can achieve parameterization with much lower angle distortion and were shown to be identical in [CSD02]. More recently, Mullen et. al. [MYAD08] presented a spectral approach to reduce common artifacts of [LPRM02, DMA02] due to positional constraints or mesh sampling irregularity and high-quality conformal parameterization can be achieved. A local/global method was proposed in [LZX*08] to build global mapping while preserving local shape properties by using transformations taken from a restricted set, which can significantly reduce both angle and area distortions.

Mesh parameterization can also be achieved by optimizing some energy form which measures the mapping distortions. Angle based flattening [SdS01] computes the parameterization which minimizes the differences between the corner angles of faces on the original mesh and their images on the parameter plane. The computational efficiency of this method is largely improved by later works in [SLMB05, ZLS07]. To further reduce distortion, the original mesh may be cut into small pieces as in [SSGH01, SCOGL02].

Since planar parameterization can be treated as finding a certain mesh metric such that the curvature is nearly 0 everywhere except singular vertices, [BCGB08] proposed a method to scale the mesh metric according to curvature specification. Our generalized Ricci flow method is also based on metric deformation, we will discuss the most related metric deformation based parameterization methods in the next sub-section.

2.2. Curvature flow

The theory of intrinsic curvature flows originated from differential geometry, and was later introduced into the engineering fields. In this section, we give a brief overview of the literature that are directly related to discrete surface curvature flow.

The Ricci flow was introduced by R. Hamilton in a seminal paper [Ham82] for Riemannian manifolds of any dimension for the purpose of proving Poincaré conjecture.

Circle packing metric was introduced by Thurston in [Thu80]. Thurston also conjectured in [Thu85] that for a discretization of the Jordan domain in the plane, the sequence of circle packings converge to the Riemann mapping. This was proved by Rodin and Sullivan [RS87]. Collins and Stephenson [CS03] implemented the computational algorithm.

In [CL03], Chow and Luo introduced the discrete Ricci flow and discrete Ricci energy on surfaces. The algorithmic implementation of the discrete Ricci flow was carried out by Jin et. al. [JKLG08]. Bowers and Stephenson [BS04b] introduced inversive distance circle packing and it was used for disk-like mesh flattening purpose in [BH03]. Guo proved the local rigidity for Euclidean and Hyperbolic inversive distance circle packing in [Guo09].

Circle pattern was proposed by Bowers and Hurdal [BH03], and has been proven to be a minimizer of a convex energy by Bobenko and Springborn [BS04a]. An efficient circle pattern algorithm was developed by Kharevych et. al. [KSS06].

In [Luo04], Luo studied the discrete Yamabe flow on surfaces. Springborn et. al. [SSP08] identified the Yamabe energy introduced by Luo with the Milnor-Lobachevsky function and the heat equation for the curvature evolution with the cotangent Laplace equation.

3. Theoretic Background

The theoretic foundation for Ricci flow on smooth surfaces has been laid down by Hamilton [Ham88] and Chow [Cho91]. In this section, smooth surface Ricci flow is generalized to the discrete setting. We briefly introduce the most related theories, for details, we refer readers to [GY07] for thorough treatments.

Suppose $M(V,E,F)$ is a simplical complex (triangle mesh) with vertex set V, edge set E and face set F respectively. We use v_i to denote the vertex, $[v_i,v_j]$ the edge connecting v_i and v_j, $[v_i,v_j,v_k]$ the face formed by v_i,v_j and v_k.

Definition 3.1 (Background Geometry) We say M is with a Euclidean $\mathbb{E}^2$ (Hyperbolic $\mathbb{H}^2$) background geometry, if each face is a Euclidean (Hyperbolic) triangle.

In both cases, the discrete metric is defined as edge length satisfying triangle inequality.

Definition 3.2 (Discrete Metric) A discrete metric on M is a function $l : E \to \mathbb{R}^+$, such that on each face $[v_i,v_j,v_k]$, the triangle inequality holds

$$l_{ij} + l_{jk} > l_{ki}.$$

The corner angles are determined by the discrete metric by Euclidean (Hyperbolic) cosine law:

$$\theta_i = \begin{cases} \arccos \frac{l_{ij}^2+l_{ki}^2-l_{ij}^2}{2l_{ij}l_{ki}} & \mathbb{E}^2 \\ \arccos \frac{\cosh l_{jk}-\cosh l_{ij}\cosh l_{ki}}{\sinh l_{ij}\sinh l_{ki}} & \mathbb{H}^2 \end{cases} \tag{1}$$

The discrete Gaussian curvature is defined as angle deficiency,

Definition 3.3 (Discrete Curvature) Suppose v_i is an interior vertex, with surrounding faces $[v_i,v_j,v_k]$. The corner angle in $[v_i,v_j,v_k]$ at the vertex v_i is denoted as θ_i^{jk} (or θ_i). Then the discrete curvature of v_i is given by

$$K_i = \begin{cases} 2\pi - \sum_{j,k}\theta_i^{jk} & v_i \notin \partial M \\ \pi - \sum_{j,k}\theta_i^{jk} & v_i \in \partial M \end{cases} \tag{2}$$

where ∂M denotes the boundary of the mesh.

Similar to the smooth case, the total curvature is determined by the topology of the mesh and the background geometry:

$$\sum_i K_i + \lambda \sum_k A_k = 2\pi\chi(M),$$

where $\chi(M) = |V| + |F| - |E|$ is the Euler number of M, λ is 0 if M is with $\mathbb{E}^2$ background geometry, λ is -1 if M is with $\mathbb{H}^2$ background geometry, A_k is the area of the k-th face.

3.1. Inversive Distance Discrete Ricci Flow

A circle packing is to associate each vertex with a circle. The circle at vertex v_i is denoted as c_i. There are two situations.

1. In Fig. 3, the two circles c_i and c_j on an edge $[v_i, v_j]$ intersect each other, the intersection angle ϕ_{ij} is acute, this is called *Andreev-Thurston circle packing*.
2. In Fig. 6, the two circles c_i and c_j on an edge $[v_i, v_j]$ are disjoint, this is called *Inversive distance circle packing*.

In both cases, the inversive distance is defined as

Definition 3.4 (Inversive Distance) Suppose the length of $[v_i, v_j]$ is l_{ij}, the radii of c_i and c_j are γ_i and γ_j respectively, then the inversive distance between c_i and c_j is given by

$$I(c_i, c_j) = \begin{cases} \frac{l_{ij}^2 - \gamma_i^2 - \gamma_j^2}{2\gamma_i\gamma_j} & \mathbb{E}^2 \\ \frac{\cosh l_{ij} - \cosh\gamma_i \cosh\gamma_j}{\sinh\gamma_i \sinh\gamma_j} & \mathbb{H}^2 \end{cases} \tag{3}$$

For Andreev-Thurston circle packing in $\mathbb{E}^2$ and $\mathbb{H}^2$, $I(c_i, c_j)$ is exactly $\cos\phi_{ij}$.

Definition 3.5 (Inversive Distance Circle Packing Metric) An inversive distance circle packing metric on a mesh M is to associate each vertex v_i with a circle c_i, whose radius is γ_i, associate each edge $[v_i, v_j]$ with a non-negative number I_{ij}. The edge length is given by

$$l_{ij} = \begin{cases} \sqrt{\gamma_i^2 + \gamma_j^2 + 2I_{ij}\gamma_i\gamma_j} & \mathbb{E}^2 \\ \cosh^{-1}(\cosh\gamma_i \cosh\gamma_j + I_{ij}\sinh\gamma_i \sinh\gamma_j) & \mathbb{H}^2 \end{cases} \tag{4}$$

The inversive distance circle packing metric is denoted as (Γ, I, M), where $\Gamma = \{\gamma_i\}$, $I = \{I_{ij}\}$.

A *discrete conformal deformation* is to change radii γ_i's only, and preserve inverse distance I_{ij}'s. The discrete Ricci flow is defined as follows:

Definition 3.6 (Discrete Ricci Flow) Given an inverse distance circle packing metric (Γ, I, M), the discrete Ricci flow is

$$\frac{du_i}{dt} = \bar{K}_i - K_i, \tag{5}$$

where

$$u_i = \begin{cases} \log\gamma_i & \mathbb{E}^2 \\ \log\tanh\frac{\gamma_i}{2} & \mathbb{H}^2 \end{cases} \tag{6}$$

$\bar{K}_i$ is the user defined target curvature on mesh vertex v_i.

Given a triangle $[v_i, v_j, v_k]$ with a inversive distance circle packing, there exists a unique circle c, which is orthogonal to c_i, c_j, c_k, shown as the red circles in Fig. 3 and Fig. 6. The center of c is O. The distance from O to edge $[v_i, v_j]$ is denoted as h_k, the edge length of $[v_i, v_j]$ is denoted as l_k.

Lemma 3.7 The following symmetric relation holds for generalized discrete Ricci flow in $\mathbb{E}^2$ (proof can be found in Appendix):

$$\frac{\partial\theta_i}{\partial u_j} = \frac{\partial\theta_j}{\partial u_i} = \frac{h_k}{l_k}. \tag{7}$$

and

$$\frac{\partial\theta_i}{\partial u_i} = -\frac{\partial\theta_i}{\partial u_j} - \frac{\partial\theta_i}{\partial u_k} \tag{8}$$

Lemma 3.8 The following symmetric relation holds for hyperbolic Ricci flow

$$\frac{\partial\theta_i}{\partial u_j} = \frac{\partial\theta_j}{\partial u_i},$$

albeit with a more complex formula. On one face $[v_1, v_2, v_3]$,

$$\begin{pmatrix} d\theta_1 \\ d\theta_2 \\ d\theta_3 \end{pmatrix} = \frac{-1}{\sin\theta_1 \sinh l_2 \sinh l_3} M \begin{pmatrix} du_1 \\ du_2 \\ du_3 \end{pmatrix} \tag{9}$$

$$M = \begin{pmatrix} 1-a^2 & ab-c & ca-b \\ ab-c & 1-b^2 & bc-a \\ ca-b & bc-a & 1-c^2 \end{pmatrix} \Lambda \begin{pmatrix} 0 & ay-z & az-y \\ bx-z & 0 & bz-x \\ cx-y & cy-x & 0 \end{pmatrix}$$

$$\Lambda = \begin{pmatrix} \frac{1}{a^2-1} & 0 & 0 \\ 0 & \frac{1}{b^2-1} & 0 \\ 0 & 0 & \frac{1}{c^2-1} \end{pmatrix}$$

where $(a, b, c) = (\cosh l_1, \cosh l_2, \cosh l_3)$, $(x, y, z) = (\cosh\gamma_1, \cosh\gamma_2, \cosh\gamma_3)$.

The detailed proof of the above lemma can be found in [Guo09].

Let $\mathbf{u}$ represent the vector $(u_1, u_2, \cdots u_n)$, $\mathbf{K}$ represent the vector $(K_1, K_2, \cdots, K_n)$, where $n = |V|$. Fixing the inversive distances, all possible $\mathbf{u}$'s that ensure the triangle inequality on each face form the *admissible metric space* of M. The above lemmas prove that the differential 1-form $\omega = \sum_i K_i du_i$ in the admissible metric space of M is a closed 1-form. The *discrete Ricci energy*

$$E(\mathbf{u}) = \int_{\mathbf{u}_0}^{\mathbf{u}} \sum_i (\bar{K}_i - K_i) du_i \tag{10}$$

is well defined, where $\mathbf{u_0} = (0, 0, \cdots, 0)$. The discrete Ricci flow (Eq. 5) is the negative gradient flow of the Ricci energy.

Theorem 3.9 (Convexity of Ricci Energy) The discrete Euclidean Ricci energy is convex on the hyper plane $\sum_i u_i = 0$ in the admissible metric space. The discrete hyperbolic Ricci energy is convex in the admissible metric space.

The basic idea to prove the above theorem is as follows. Based on Lemma 3.7 and 3.8, it can be proved that the Jacobian matrix of functions θ_1, θ_2, θ_3 in terms of u_1, u_2, u_3 has one zero eigenvalue with associated eigenvector $(1, 1, 1)$ and two negative eigenvalues. Then the differential 1-form $\sum_{i=1}^3 \theta_i du_i$ is closed, the integration $\omega(u_1, u_2, u_3) = \int_{(u_1^0, u_2^0, u_3^0)}^{(u_1, u_2, u_3)} \sum_{i=1}^3 \theta_i du_i$ is a concave function. Then by taking

sum of all the 1-forms within each mesh triangle and according to Eq. 2, the convexity of discrete Ricci energy can be proved. The details of the proof can be found in [CL03], [Guo09] and [GY08]. Then we know that the metric producing the target curvature is the unique global optimum of the Ricci energy. Therefore, discrete Ricci flow won't get stuck at the local optimum, and converges to the global optimum.

4. Generalized Discrete Ricci Flow Algorithm

This section introduces the practical algorithms of computing mesh parameterization based generalized Ricci flow.

4.1. Compute the Initial Circle Packing Metric

Given a triangle mesh, the inversive distance circle packing metric which exactly equals to the original Euclidean mesh metric is computed as follows:

1. For each face $[v_i, v_j, v_k]$, we compute
$$\gamma_i^{jk} = \frac{l_{ij} + l_{ki} - l_{jk}}{2}.$$
2. For each vertex v_i, the radius of c_i is given by
$$\gamma_i = \min_{jk} \gamma_i^{jk}.$$
3. For each edge $[v_i, v_j]$, the inversive distance is given by Eq. 3.

4.2. Optimize Ricci Energy

After the initial inversive distance circle packing metric is set, the conformal metric which induces user prescribed target curvature $\bar{K_i}$ is computed by:

1. For each edge $[v_i, v_j]$, using current radii γ_i, γ_j and inversive distance I_{ij}, compute the current edge length l_{ij} by Eq. 4.
2. For each face $[v_i, v_j, v_k]$, using the current edge length to compute the corner angles $\theta_i, \theta_j, \theta_k$ by Eq. 1.
3. For each vertex v_i, compute the current curvature K_i using Eq. 2.
4. For each face $[v_i, v_j, v_k]$, compute $\frac{\partial \theta_i}{\partial u_j}$ and $\frac{\partial \theta_i}{\partial u_i}$ using Eq. 7, 8 or Eq. 9.
5. Form the Hessian matrix Δ of the discrete Ricci energy in Eq. 10. It is easy to verify from Eq. 2 and Eq. 10 that the Hessian matrix has an explicit form $\Delta = (h_{ij})$:
$$h_{ij} = \begin{cases} -w_{ij} & i \neq j, [v_i, v_j] \in E \\ \sum_k w_{ik} & i = j, [v_i, v_k] \in E \\ 0 & i \neq j, [v_i, v_j] \notin E \end{cases} \quad (11)$$
where
$$w_{ij} = \frac{\partial \theta_i^{jk}}{\partial u_j} + \frac{\partial \theta_i^{jl}}{\partial u_j}. \quad (12)$$
6. Solve the following linear system
$$\Delta \mu = \bar{K_i} - K_i.$$

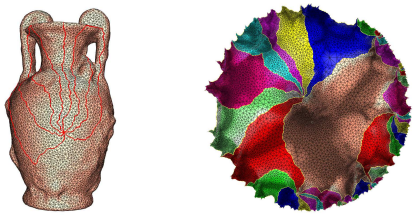

Figure 8: *Generalized hyperbolic Ricci flow on Amphora model.*

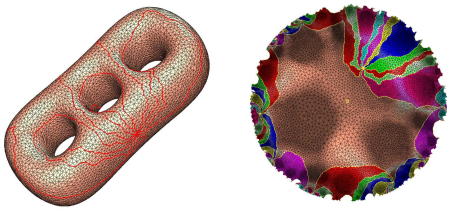

Figure 9: *Generalized hyperbolic Ricci flow on 3 holed Torus model.*

7. Update $u_i \leftarrow u_i + \mu_i$.
8. Repeat step 1 through 7, until
$$\max_i |\bar{K_i} - K_i| < \varepsilon.$$

4.3. Flattening the Mesh

For generalized Euclidean Ricci flow, after the target circle packing metric is computed, we can use Eq. 4 to get the corresponding Euclidean metric. Then the mesh can be flattened onto the plane by the following simple algorithm.

1. Compute a homology group basis [EW05], cut the surface open along the base curves. Denote the open mesh as $\bar{M}$.
2. Using Euclidean cosine law, flatten each triangle in $\bar{M}$ isometrically on the plane.
3. Using rigid motion to glue the embedded faces of $\bar{M}$ together.

For generalized hyperbolic Ricci flow, there are several key differences to flatten the mesh compared with Euclidean case. First, we embed the mesh onto the Poincaré disk instead of the plane. Second, the embedding of each triangle is based on hyperbolic cosine law, instead of Euclidean cosine law. Third, for gluing of different embedded triangles, the rigid motions are hyperbolic rigid motions, instead of Euclidean ones. We refer readers to [JKLG08] for more details. Fig. 8 and Fig. 9 show two high genus models parameterized using hyperbolic inversive distance Ricci flow.

5. Experiments

In this section, we test our generalized Ricci flow algorithm on variant models with low quality triangulations to show

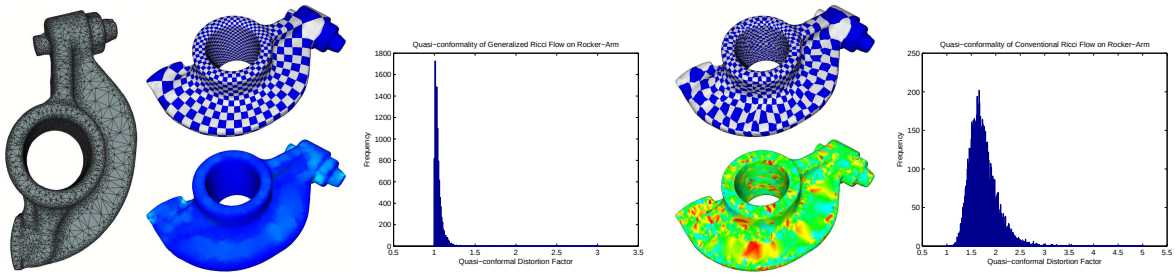

(a) (b) (c) (d) (e)

Figure 10: *Conformality comparison on Rock-Arm model. a) The original model with low quality triangulation. b) Generalized Ricci flow result and color coded QC distortion. c) The histogram of QC distortion on mesh vertices using generalized Ricci flow. d) Conventional Ricci flow result and color coded QC distortion. e) The histogram of QC distortion using conventional Ricci flow.*

the good conformality, flexibility and robustness of the parameterization results.

5.1. Conformality

Due to the exact equality between the original Euclidean metric and the inversive distance circle packing metric, our generalized Ricci flow method results in parameterization with good conformality compared with the conventional Ricci flow method. To quantitatively measure the conformality, we adapt the quasi-conformal(QC) distortion [SSGH01]. The distortion factor is computed within mesh triangle face as the ratio of larger to smaller eigenvalues of the Jacobian of the map. The ideal conformality is 1, larger value for worse conformality. The color coded map is rendered based on the area weighted distortion on each mesh vertex, blue for 1, red for largest distortion value of generalized Ricci flow method. The conformality comparison result on Rocker-Arm model with low quality triangulation is shown in Fig. 10. Since the original model is genus 1 boundary 0, we set the target curvature to 0 for all vertices. For traditional Ricci flow method, we force all the intersection angles ϕ_{ij} to be acute, this compromises the conformality. From the visual effect of the checker board texture mapping, we can easily find that the generalized Ricci flow can get results with much better conformality. This is also verified by the color-coded map of QC distortion. The histogram also shows that the QC distortion factors highly concentrate to 1 in generalized Ricci flow case, while the conventional Ricci flow result diverges much more. More results using generalized Ricci flow with good conformality will be presented later, and the average QC factors are listed in Table 1.

5.2. Flexibility

As the previous curvature flow based method [JKLG08] [SSP08], our method is capable of computing the conformal parameterization with arbitrary user prescribed target curvatures. Fig. 11 shows the results of a frog model of genus 0 and boundary 1. From Gauss-Bonnet theorem, the sum of

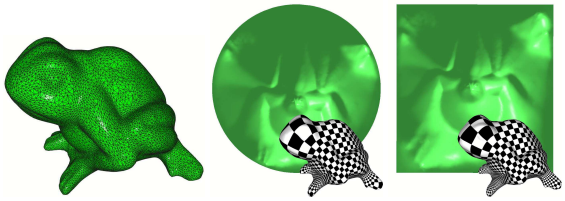

(a) (b) (c)

Figure 11: *Flexible boundary curvature specification of generalized Ricci flow. a) The original model with low quality triangulation. b) Circular boundary parameterization. c) Rectangular boundary parameterization.*

target curvature on mesh vertex is 2π. After setting all inner mesh vertex target curvature to 0, the boundary vertex curvature can be assigned proportional to its length within the whole boundary, then we can get the circular conformal parameterization as shown in Fig. 11(b). If a rectangular parameter domain is needed, we can choose four boundary vertices and make the target curvature equal to $\pi/2$ and set all other mesh vertex curvature to 0. The corresponding result is shown in Fig. 11(c).

5.3. Set the Boundary Free

After setting the initial circle packing metric based on inversive distance, we can leave the boundary as it is and only optimize the metric of the inner part, which means we set $du_i = 0$ on boundary vertices. This leads to the so-called free boundary Ricci flow which preserves the original metric on mesh boundaries. Since there is no constraint on the mesh boundary, the area distortion of the parameterization will be effectively minimized [YKL*08] [SSP08]. Fig. 12 shows an example on Nicolo da Uzzano model.

(a) (b) (c)

Figure 12: *Free boundary generalized Ricci flow on Nicolo da Uzzano model. a) The original model with low quality triangulation. b) The embedded parameter domain. c) The parameterization result with texture mapping.*

5.4. Preserve Triangle Inequality

During the optimization process of the generalized Ricci flow, the circle packing metric is updated because the vertex radius changes. This means the induced Euclidean metric is also changed. There is a possibility that the Euclidean triangle inequality would be violated (also see [SSP08]). Edge swap (for inner edge) or splitting (for boundary edge) is necessary to help to achieve the global optimum. The edge swap is performed on mesh edge whose length is larger than the sum of the other two edges' within a mesh face. During edge swap, we maintain the circle radii on the swapped edge vertices. For the new edge, the corresponding inversive distance is computed from the original Euclidean distance of the two edge vertices of the mesh. Edge split is needed if the edge lies on mesh boundary. In this rare case, the inversive distance circle packing metric needs to be re-initialized. Fig. 13 shows a Buste model with base cut and an inner boundary sliced on the head. Since it is genus 0 and boundary 2, we set target curvature to 0 everywhere. Five mesh edges are swapped to maintain the triangle inequality and the generalized Ricci flow can be optimized. For other test cases in our paper, only Nicolo da Uzzano model needs 6 edge swaps and no boundary edge split is observed during the experiments.

5.5. Performance and Discussions

Our generalized Ricci flow algorithm is implemented in C++ on a PC with Intel Q9400 CPU of 2.66 GHz and 2GB RAM. And we use Matlab C++ library to solve the sparse system in Section 4.2. The computational time and average QC distortion is summarized in Table 1.

For traditional Ricci flow of Fig. 5 and Fig. 10(d), the average QC distortions are 2.3570 and 1.7405 respectively, which are much worse than the corresponding generalized Ricci flow results. Because generalized Ricci flow based on inversive distance is also a convex energy optimization, it can be efficiently computed using Newton's method as in Section 4.2. As a result, the computational efficiency is comparable to those of traditional Ricci flow.

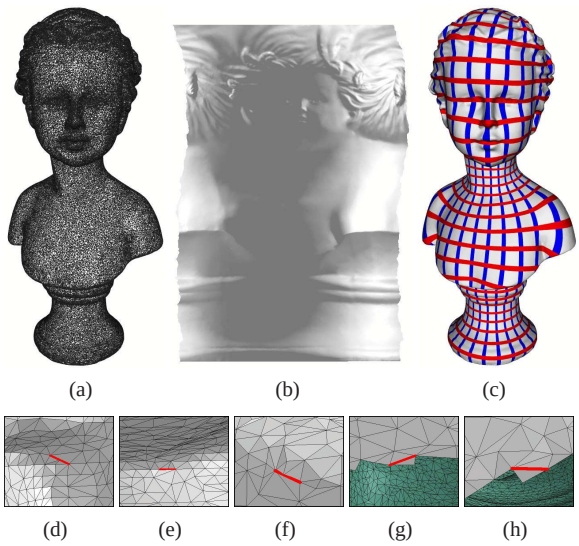

(a) (b) (c)

(d) (e) (f) (g) (h)

Figure 13: *Generalized Ricci flow on Buste model. a) The original model with low quality triangulation. b) The embedded parameter domain. c) The parameterization result with texture mapping. d ~h) Five swapped edges during flow.*

Model	|F|	Avg QC	Time(s)
Kitten	66952	1.0306	12.8
Rocker-Arm	20088	1.0461	3.8
Frog(cir.)	22856	1.0531	6.5
Frog(rect.)	22856	1.0443	5.2
Nicolo	50053	1.0220	9.4
Buste	107259	1.0294	30.6

Table 1: *Statistics of generalized Ricci flow*

Note that in the previous work [KSS06] based on circle pattern, the conformal parameterization can also be computed by a convex energy optimization. The difference is that circle pattern defined curvatures on both vertices and faces, while our generalized discrete Ricci flow method has only vertex curvatures. Furthermore, [KSS06] only focused on Euclidean case, our work also handles hyperbolic case. Compared to the metric scaling approach in [BCGB08], our parameterization result is achieved by minimizing a convex energy. In contrast, the metric scaling parameterization is based on an approximation of conformal factor estimation. There is no guarantee that a total exact flat metric can be carried out. Their work also studied Euclidean case only.

6. Conclusion

This work generalizes discrete surface Ricci flow from Andreev-Thurston circle packing to inversive distance circle packing. Conventional discrete Ricci flow method can not achieve both high stability and high conformality for meshes with low quality triangulations. The generalized Ricci flow algorithm greatly improves the robustness and the confor-

mality. It preserves the convexity of the Ricci energy as well. Therefore, the generalized Ricci flow is much more flexible, robust, and conformal. Furthermore, this work gives the geometric interpretation of the Hessian matrix of discrete Ricci energy based on inversive distance circle packing metric.

In the future, we will find the geometric interpretation of the Hessian of the hyperbolic Ricci energy. We will develop parallel generalized Ricci flow algorithm and apply it for more applications in graphics.

Acknowledgements

The models used in this paper are the courtesy of Stanford University and AIM@SHAPE shape repository. This work is partially supported by National Basic Research Project of China (Project Number 2006CB303102), the Natural Science Foundation of China (Project Number 60673004, 60628202), the National High Technology Research and Development Program of China (Project Number 2007AA01Z336), the National Science Foundation CCF-0448339, CCF-0830550, CCF-0841514 and ONR N000140910228. Ren Guo and Feng Luo are partially supported by the National Science Foundation of USA (Project Number 0625935, 0604352).

References

[BCGB08] BEN-CHEN M., GOTSMAN C., BUNIN G.: Conformal flattening by curvature prescription and metric scaling. *Computer Graphics Forum (Proc. Eurographics 2008) 27*, 2 (2008), 449–458.

[BH03] BOWERS P. L., HURDAL M. K.: Planar conformal mapping of piecewise flat surfaces. In *Visualization and Mathematics III* (Berlin, 2003), Springer-Verlag, pp. 3–34.

[BS04a] BOBENKO A. I., SPRINGBORN B. A.: Variational principles for circle patterns and koebe's theorem. *Transactions of the American Mathematical Society 356* (2004), 659–689.

[BS04b] BOWERS P., STEPHENSON K.: Uniformizing dessins and belyi maps via circle packing. *Mem.Amer.Soc. 170*, 805 (2004).

[Cho91] CHOW B.: The ricci flow on the 2-sphere. *J. Differential Geom. 33*, 2 (1991), 325–334.

[CL03] CHOW B., LUO F.: Combinatorial Ricci flows on surfaces. *Journal Differential Geometry 63*, 1 (2003), 97–129.

[CS03] COLLINS C., STEPHENSON K.: A circle packing algorithm. *Computational Geometry: Theory and Applications 25* (2003), 233–256.

[CSD02] COHEN-STEINER D., DESBRUN M.: Hindsight: Lscm and dcp are one and the same. In *www.geometry.caltech.edu/pubs/CD02.pdf* (2002).

[DMA02] DESBRUN M., MEYER M., ALLIEZ P.: Intrinsic parameterizations of surface meshes. *Computer Graphics Forum (Proc. Eurographics 2002) 21*, 3 (2002), 209–218.

[EDD*95] ECK M., DEROSE T., DUCHAMP T., HOPPE H., LOUNSBERY M., STUETZLE W.: Multiresolution analysis of arbitrary meshes. In *SIGGRAPH '95* (1995), pp. 173–182.

[EW05] ERICKSON J., WHITTLESEY K.: Greedy optimal homotopy and homology generators. In *SODA '05* (2005), pp. 1038–1046.

[FH05] FLOATER M. S., HORMANN K.: Surface parameterization: a tutorial and survey. In *Advances in Multiresolution for Geometric Modelling*. Springer, 2005, pp. 157–186.

[Flo97] FLOATER M. S.: Parametrization and smooth approximation of surface triangulations. *Comput. Aided Geom. Des. 14*, 3 (1997), 231–250.

[Flo03] FLOATER M. S.: Mean value coordinates. *Comput. Aided Geom. Des. 20*, 1 (2003), 19–27.

[Guo09] GUO R.: *Local Rigidity of Inversive Distance Circle Packing*. Tech. Rep. arXiv.org, Mar 8 2009.

[GY07] GU X., YAU S.-T.: *Computational Conformal Geometry*, vol. 3. Higher Education Press, 2007.

[GY08] GU X. D., YAU S.-T.: *Computational Conformal Geometry*. Advanced Lectures in Mathematics. High Education Press and International Press, 2008.

[Ham82] HAMILTON R. S.: Three manifolds with positive Ricci curvature. *Journal of Differential Geometry. 17* (1982), 255–306.

[Ham88] HAMILTON R. S.: The Ricci flow on surfaces. *Mathematics and general relativity (Santa Cruz, CA, 1986), Contemp. Math. Amer.Math.Soc. Providence, RI 71* (1988).

[HLS07] HORMANN K., LÉVY B., SHEFFER A.: Mesh parameterization: Theory and practice. In *ACM SIGGRAPH Course Notes* (2007).

[JKLG08] JIN M., KIM J., LUO F., GU X.: Discrete surface ricci flow. *IEEE Transactions on Visualization and Computer Graphics 14*, 5 (2008), 1030–1043.

[Ju04] JU T.: Robust repair of polygonal models. *ACM Trans. Graph. 23*, 3 (2004), 888–895.

[JZLG08] JIN M., ZENG W., LUO F., GU X.: Computing teichmüller shape space. *IEEE Transactions on Visualization and Computer Graphics 15*, 3 (2008), 504–517.

[KSS06] KHAREVYCH L., SPRINGBORN B., SCHRÖDER P.: Discrete conformal mappings via circle patterns. *ACM Trans. Graph. 25*, 2 (2006), 412–438.

[LPRM02] LÉVY B., PETITJEAN S., RAY N., MAILLOT J.: Least squares conformal maps for automatic texture atlas generation. *SIGGRAPH 2002* (2002), 362–371.

[Luo04] LUO F.: Combinatorial yamabe flow on surfaces. *Commun. Contemp. Math. 6*, 5 (2004), 765–780.

[LZX*08] LIU L., ZHANG L., XU Y., GOTSMAN C., GORTLER S. J.: A local/global approach to mesh parameterization. *Computer Graphics Forum (Proceedings of SGP 2008) 27*, 5 (2008), 1495–1504.

[MYAD08] MULLEN P., YIYING T., ALLIEZ P., DESBRUN M.: Spectral conformal parameterization. *Computer Graphics Forum (Proceedings of SGP 2008) 27*, 5 (2008), 1487 – 1494.

[PP93] PINKALL U., POLTHIER K.: Computing discrete minimal surfaces and their conjugates. *Experimental Mathematics 2* (1993), 15–36.

[RS87] RODIN B., SULLIVAN D.: The convergence of circle packings to the riemann mapping. *Journal of Differential Geometry 26*, 2 (1987), 349–360.

[SCOGL02] SORKINE O., COHEN-OR D., GOLDENTHAL R., LISCHINSKI D.: Bounded-distortion piecewise mesh parameterization. In *IEEE Visualization* (2002), pp. 355–362.

[SdS01] SHEFFER A., DE STURLER E.: Parameterization of faced surfaces for meshing using angle based flattening. *Engineering with Computers 17*, 3 (2001), 326–337.

[SLMB05] SHEFFER A., LÉVY B., MOGILNITSKY M., BOGOMYAKOV A.: ABF++: fast and robust angle based flattening. *ACM Transactions on Graphics 24*, 2 (2005), 311–330.

[SPR06] SHEFFER A., PRAUN E., ROSE K.: *Mesh Parameterization Methods and Their Applications*, vol. 2 of *Foundations and Trends in Computer Graphics and Vision*. Now Publisher, 2006.

[SSGH01] SANDER P. V., SNYDER J., GORTLER S. J., HOPPE H.: Texture mapping progressive meshes. In *SIGGRAPH '01* (2001), pp. 409–416.

[SSP08] SPRINGBORN B., SCHRÖDER P., PINKALL U.: Conformal equivalence of triangle meshes. *ACM Transactions on Graphics 27*, 3 (2008), 1–11.

[Thu80] THURSTON W. P.: *Geometry and Topology of Three-Manifolds*. lecture notes at Princeton university, 1980.

[Thu85] THURSTON W. P.: The finite riemann mapping theorem.

[Tut63] TUTTE W. T.: How to draw a graph. *Proc. London Math 13* (1963), 743–768.

[xHS96] XU HE Z., SCHRAMM O.: On the convergence of circle packings to the riemann map. *Invent. Math 125* (1996), 285–305.

[YKL*08] YANG Y.-L., KIM J., LUO F., HU S.-M., GU X.: Optimal surface parameterization using inverse curvature map. *IEEE Transactions on Visualization and Computer Graphics 14*, 5 (2008), 1054–1066.

[ZJLG09] ZENG W., JIN M., LUO F., GU X.: Canonical homotopy class representative using hyperbolic structure. In *Proc. of IEEE Interantaional Conference on Shape Modeling and Applications (SMI)* (2009).

[ZLS07] ZAYER R., LÉVY B., SEIDEL H.-P.: Linear angle based parameterization. In *Symposium on Geometry Processing* (2007), pp. 135–141.

Appendix: Geometry Interpretation of the Hessian Matrix of Discrete Euclidean Ricci Energy

We now prove Eq. 7 in Lemma 3.7. We use the same notations of inversive distance circle packing metric as in Section 3. For simplicity, we use l_k instead of l_{ij} to denote the length of mesh edge $[v_i, v_j]$.

Lemma 6.1 Given a Euclidean triangle with Inversive distance circle packing metric, we have

$$\gamma_i \frac{\partial l_k}{\partial \gamma_i} = \frac{l_k^2 + \gamma_i^2 - \gamma_j^2}{2l_k}. \tag{13}$$

Proof: It can be easily proved by simply taking $\frac{\partial}{\partial \gamma_i}$ to both sides of Eq. 4 in Euclidean case. This is also true for Andreev-Thurston circle packing.□

Lemma 6.2 Given a Euclidean triangle as in Fig. 14, then

$$R_{i,j} = \frac{l_k^2 + \gamma_i^2 - \gamma_j^2}{2l_k}. \tag{14}$$

Proof: Obviously, we have $\gamma_i^2 - R_{i,j}^2 = \gamma_j^2 - (l_k - R_{i,j})^2 = t^2$. Then it can be proved by simple computation. □

Note that by applying Lemma 6.1, for Andreev-Thurston circle packing, we have

$$\gamma_i \frac{\partial l_k}{\partial \gamma_i} = R_{i,j}. \tag{15}$$

For Inversive distance circle packing as in Fig. 15(a), although the circles may not intersect with each other, we can consider $\triangle v_i v_j O$ instead. Then $R_{i,j} = \frac{1}{2l_k}(l_k^2 + x_i^2 - x_j^2)$. Let Υ be the radius of the circle perpendicular to all 3 circles c_i, c_j, c_k, then we have $x_i^2 = \gamma_i^2 + \Upsilon^2$, $x_j^2 = \gamma_j^2 + \Upsilon^2$. This means Eq. 15 is also true for Inversive distance case.

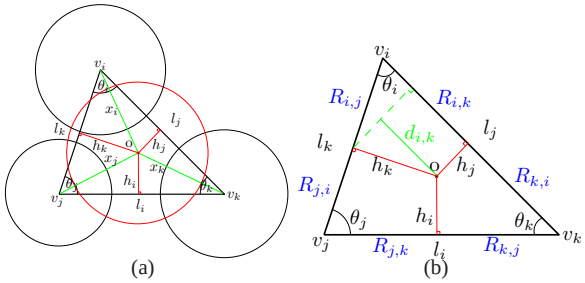

Figure 15: *Inversive distance circle packing.*

To prove Lemma 3.7, we don't treat two types of circle packing metric separately because the situations are the same. Suppose A is the area of triangle face $[v_i, v_j, v_k]$, it is well known that the following equation holds:

$$\frac{\partial \theta_i}{\partial l_i} = \frac{l_i}{2A}. \tag{16}$$

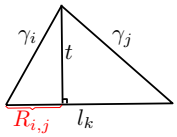

Figure 14: *Euclidean Triangle.*

Then we have:

$$\frac{\partial \theta_j}{\partial \gamma_i} = \frac{\partial \theta_j}{\partial l_j}\frac{\partial l_j}{\partial \gamma_i} + \frac{\partial \theta_j}{\partial l_k}\frac{\partial l_k}{\partial \gamma_i}.$$

By applying derivative cosine law to the above equation,

$$\frac{\partial \theta_j}{\partial \gamma_i} = (\frac{\partial \theta_j}{\partial l_j})[\frac{\partial l_j}{\partial \gamma_i} - \frac{\partial l_k}{\partial \gamma_i}\cos\theta_i].$$

Then from Eq. 15 and Eq. 16, we have:

$$\begin{aligned} \gamma_i \frac{\partial \theta_j}{\partial \gamma_i} &= (\frac{\partial \theta_j}{\partial l_j})[\gamma_i \frac{\partial l_j}{\partial \gamma_i} - \gamma_i \frac{\partial l_k}{\partial \gamma_i}\cos\theta_i] \\ &= \frac{l_j}{2A}[R_{i,k} - R_{i,j}\cos\theta_i] \\ &= \frac{l_j}{2A}\cdot d_{i,k}. \end{aligned}$$

From Fig. 15(b), we can easily find that $\frac{d_{i,k}}{h_k} = \sin\theta_i$. Thus,

$$\frac{\partial \theta_j}{\partial u_i} = \frac{\partial \theta_j}{\partial (\ln \gamma_i)} = \frac{l_j}{2A}\cdot h_k \cdot \sin(\theta_i) = \frac{l_j \sin\theta_i}{l_j l_k \sin\theta_i}\cdot h_k = \frac{h_k}{l_k}.$$

The above proof is also true for $\frac{\partial \theta_i}{\partial u_j}$.

It is easy to prove Eq. 8 in Lemma 3.7. For a mesh face $[v_i, v_j, v_k]$, we have $\theta_i + \theta_j + \theta_k = \pi$. Then we have $\frac{\partial \theta_i}{\partial u_i} + \frac{\partial \theta_j}{\partial u_i} + \frac{\partial \theta_k}{\partial u_i} = 0$. By applying the symmetry relation in Eq. 7, Eq. 8 can be proved. □